

Two-Band Superconductivity in MgB₂

M. Iavarone, G. Karapetrov, A. E. Koshelev, W. K. Kwok, G. W. Crabtree, and D. G. Hinks
Materials Science Division, Argonne National Laboratory, Argonne, Illinois 60439
 (October 31, 2018)

The study of the anisotropic superconductor MgB₂ using a combination of scanning tunneling microscopy and spectroscopy reveals two distinct energy gaps at $\Delta_1=2.3$ meV and $\Delta_2=7.1$ meV. Different spectral weights of the partial superconducting density of states (PDOS) are a reflection of different tunneling directions in this multi-band system. Our experimental observations are consistent with the existence of two-band superconductivity in the presence of interband superconducting pair interaction and quasiparticle scattering. Temperature evolution of the tunneling spectra follows the BCS scenario [1] with both gaps vanishing at the bulk T_c . Indeed, the study of tunneling junctions exhibiting only the small gap (*c*-axis tunneling) clearly and reproducibly show that this gap persists up to the bulk T_c . The data confirm the importance of Fermi-surface sheet dependent superconductivity in MgB₂ proposed in the multigap model by Liu et al. [2].

The discovery of superconductivity in MgB₂ [3] at 39K sparked great interest in the fundamental physics and practical applications of this material. There has already been rapid progress in understanding the physical properties of this superconductor. Specific heat measurements [4,5] show that MgB₂ is an s-wave superconductor and the presence of the isotope effect [6,7] points towards phonon-mediated pairing. Tunneling and photoemission spectroscopy directly measures the superconducting energy gap and can provide further understanding of the origin of the superconductivity in this material. Earlier tunneling spectroscopy measurements show a large spread in the gap values [8–10] each consistent with the BCS form. More recent experiments, including STM tunneling spectroscopy [11], point-contact spectroscopy [12,13], specific heat measurements [4,5], and Raman spectroscopy [14] point towards the existence of two distinct gaps. This scenario has been predicted theoretically by Liu et al. [2]. First principle calculations show that the Fermi surface of MgB₂ consists of 2D cylindrical sheets arising from σ antibonding states of B p_{xy} orbitals, and 3D tubular networks arising from π bonding and antibonding states of B p_z orbitals. In this theoretical framework [2] two different energy gaps exist, the smaller one being an induced gap associated with the 3D bands and the larger one associated with the superconducting 2D bands. Furthermore both superconducting gaps should vanish at the bulk critical temperature T_c . Due to this highly anisotropic band structure the superconducting gaps should be momentum-dependent reflecting the strength of the electron-phonon coupling of the carriers in the different bands. Up to now there has been no direct experimental evidence of the orientation dependence of the order parameter in this material. Moreover, the temperature dependence of the two gaps would give further insights into the nature of superconductivity in MgB₂. Scanning tunneling spectroscopy is a unique technique that allows direct measure of the

DOS near the Fermi energy with high spatial and energy resolution. Since the tunneling current couples only to bands with an appreciable Fermi velocity in the tunneling direction STM can distinguish between the 2D bands with little or no *c*-axis component of Fermi velocity and 3D bands with considerable *c*-axis component. Thus, in the clean limit ($l \gg 2\pi\xi$) the direction of the tunneling current selects which band and which superconducting gap is probed. In this paper we report direct evidence of orientation-dependent double-gap structure in the quasi-particle energy spectra as determined from tunneling spectroscopy. Our data are consistent with the theoretical predictions of multigap superconductivity in the clean limit. Temperature dependent tunneling shows that the two distinct gaps vanish simultaneously near the bulk T_c .

Compact samples of MgB₂ were synthesized from amorphous B powder (4N's purity) and high purity Mg. The B powder was pressed into pellets under 6 kbar pressure. These pellets were reacted with Mg vapor at 850 C for 2 hr in a BN container under 50 bar of Ar. During the reaction the pellets broke up in pieces of several mm in size. The typical critical temperature of these gold-colored pellets is 39K.

The tunneling measurements were performed on these samples using different surface preparation methods. One procedure consisted of chemically etching the pellets for 50 seconds in bromine (Br 1% in pure ethanol), then rinsing in pure ethanol and drying in N₂ gas. Alternative procedures consisted of cleaving or mechanical polishing of the sample in an inert atmosphere. After these treatments the samples were mounted on the STM stage in He exchange gas and cooled down to 4.2 K. These procedures all yielded equivalent tunneling results. The measurements were performed with a home-built STM described elsewhere [8].

The typical conductance spectra recorded on different grains within the sample are shown in Figure 1. The

typical grain size is of the order of 50 nm and the spectra are remarkably reproducible within the same grain both with respect to location and tunneling resistance. All the spectra are normalized to the conductance value at -20mV . They reveal a double gap structure, flat background, and very low zero-bias conductance with very little broadening other than thermal smearing. Two peaks are present at $V_1 \sim 3\text{ mV}$ and $V_2 \sim 7.5\text{ mV}$, symmetrically for both injection and emission of electrons and they stay within 10% of these values when changing between grains and/or samples. This gap size distribution is in line with the proposed distribution of the gap values over the Fermi surface by Choi et al. [15].

Figure 2(a) is the representative surface topography (150 nm x 150 nm) showing several different grains. The roughness within an individual grain is about 1nm and the grains are separated by steps that are 1-10nm high. Each of the four grains is characterized by a tunneling spectrum that is consistent within a particular grain. Within this scanning area we focus on the tunneling spectra acquired on grains 1 and 2 (Fig. 2a). The spectrum recorded in grain 2 shows a clear two-gap structure dominated by the high-energy gap while in grain 1 only the smaller gap is pronounced and the high-energy peak becomes a weak satellite feature. The main characteristics of the spectra, including the spectral weight of each peak, do not change with the tunneling resistance from 0.1 to 2 G Ω . Having this remarkable spatial reproducibility of the tunneling conductance we focus our attention on the origin of the different spectra in these grains. First, we point out that both spectra are in agreement with the multi-gap scenario proposed by Liu et al. [2] where in the clean limit the impurity and surface scattering do not significantly influence the spectra. Second, we find a striking similarity between the spectrum in grain 1 and the typical spectrum we recorded earlier on c-axis oriented films [16]. In the c-axis tunneling on MgB₂ epitaxial films the contribution from the 3D Fermi surface is expected to dominate the tunneling conductance. Thus we believe that the distinct spectra attributable to grain 1 and 2 are a reflection of different crystallographic grain orientation with respect to the tunneling direction. This evidence of momentum-dependent tunneling is further supported by the spatial and temperature-dependent analysis of the spectra presented below.

To elucidate the origin of the different spectra in the two grains we studied the spatial evolution of the spectra across the grain boundary. In Figure 2(b,c) we show the conductance maps at the superconducting peak values of $V_1=+3.3\text{ mV}$ and $V_2=+7.3\text{ mV}$ in the region indicated by the square spanning the two grains. In these maps the bright zones mark regions where the tunneling spectra show higher conductance at the energy corresponding to V_1 (Fig. 2(b)) or V_2 (Fig. 2(c)), respectively. The transition from one type of spectra to the other evolves over a length scale on the order of 5 nm. We associate these

two different types of spectra with vacuum tunneling into grains with two distinct orientations. The smooth transition between the spectra across the grain boundary on *the length scale of ξ* is further evidence of the sample being in the clean limit.

The distinct tunneling conductance spectra that we observe are consistent with the two-gap BCS model [17] taking into account interband impurity scattering (see, e.g., [18]). According to this model the partial densities of states (PDOS) of two bands $N_{1(2)}(\omega)$

$$N_{1(2)}(\omega) = N_{1(2)}(0) \text{Re} \left[\frac{u_{1(2)}}{\sqrt{u_{1(2)}^2 - 1}} \right],$$

are determined by two dimensionless functions $u_{1(2)}(\omega)$ that obey equations

$$\begin{aligned} u_1 \Delta_1 &= \omega + i\Gamma + i\Gamma_{12} \frac{u_2 - u_1}{\sqrt{u_2^2 - 1}}, \\ u_2 \Delta_2 &= \omega + i\Gamma + i\Gamma_{21} \frac{u_1 - u_2}{\sqrt{u_1^2 - 1}}. \end{aligned}$$

Here $\Delta_{1,2}$ are the gap parameters of two bands, Γ_{12} and Γ_{21} are the interband scattering rates, with $\Gamma_{12}/\Gamma_{21} = N_2(0)/N_1(0)$. It is important to note that strong interband scattering suppresses the superconducting transition temperature. In particular, at $\Gamma_{21} \ll T_c$ and $\Delta_1 \ll \Delta_2$, $\delta T_c \approx -\pi\Gamma_{21}/8$ (see, e. g., [19]).

We use a linear combination of the two PDOS to obtain the total DOS

$$N_{tot}(\omega) = \alpha N_1(\omega) + \beta N_2(\omega)$$

that we compare with the experimental tunneling conductance spectra. The PDOS' spectral weight represented by the parameters α and β ($\alpha+\beta=1$) is associated with the relative orientation of the crystallographic axis of a grain with respect to the tunneling barrier. Thus in the fits shown below the parameters α and β are kept constant for all spectra obtained on a particular grain at different temperatures.

The linear combination of the two PDOS shown above accounts for all major features in our tunneling spectra including the temperature dependent data. The evolution of the tunneling spectra in the temperature range between 4.2K and 42K are displayed in Figure 3. The two-gap signature in the spectra of grain 1 becomes hardly distinguishable with increasing the temperature (Fig. 3(a)). The small gap shows a rapid decrease in the peak height and the conductance peaks of the two gaps merge into a broad peak at $T \approx 10\text{K}$. In order to separate the temperature evolution of each PDOS we used the temperature dependence of the spectrum on grain 2 (Fig. 3(b)) where only the small gap is present. Each curve was normalized to the conductance value at -20 mV and then compared with the theoretical curve at the

same temperature. The theoretical curves were obtained by fixing the interband scattering rates Γ_{12} , Γ_{21} and the smearing parameter Γ at values optimized for the 4.2 K conductance spectra. In all the fits we put $\Gamma_{12}=0.73\Gamma_{21}$ since their ratio is proportional to the ratio of the density of states at the Fermi level of the 3D and the 2D bands [18,20]. The theoretical curves reproduce very well the shape inside the gap but not the peak heights. By adjusting the parameters Γ_{12} and Γ we could reproduce very well the peak heights but the zero bias value would be higher than the experimental one. Fits to the two set of parameters have been used to get an estimate of the error bars for the two gap values: $\Delta_1=2.3\pm 0.2$ mV and $\Delta_2=7.1\pm 0.2$. A very good fit of both peaks' height and zero bias value can be obtained only for interband scattering values that are very large (~ 2.5 mV) and values of the 3D gap is extremely small. According to [19] such a large interband scattering value should lower the critical temperature by ~ 9 K which contradicts our experimental findings. The set of temperature dependent tunneling spectra clearly shows that both superconducting gaps exist up to 37K.

Next, we turn our attention to the spectral weights of the two PDOS to the total DOS. The particular choice of the two grains in Fig. 2 was based on the peculiarity of the conductance spectra of these crystallites. They closely represent the two extreme limits of partial contribution by each PDOS that we have observed so far on a large number of pellets and thin films. The theoretical fits obtained by our model in these two limits (Fig. 3a,b) show that the contribution of the 3D PDOS varies from nearly 100% (Fig. 3b and [16]) down to 87% (Fig. 3a). Therefore it appears that momentum averaged STM tunneling conductance is dominated by the 3D band in this momentum dependent two-band tunneling process. This could be due to the specific geometry of the tunneling cone emanating from the STM tip and its projection on the highly anisotropic Fermi surface of the MgB₂ crystallite. Obviously, the relative weights of the PDOS are temperature independent and the parameters α and β remain fixed when the temperature dependent fits of the tunneling spectra are obtained.

The values of $\Delta_1(T)$ and $\Delta_2(T)$ are extracted from the theoretical curves and the results are reported in Figure 3(c). The high-energy gap follows a BCS behavior. The smaller gap remains constant up to 20K and follows the BCS predictions with a critical temperature far beyond the one expected for such a small gap ($T_c \approx 14$ K) with a ratio $2\Delta/kT_c \approx 1.4$ similar to earlier findings from point spectroscopy [13]. Such behavior clearly demonstrates that the gap in the 3D band is mainly induced by the interband pairing interaction rather than produced by pairing interaction inside this band, in agreement with theoretical expectations [2,15]. This experimental evidence directly excludes the possibility that the grains or their surfaces are associated with different stoichiometry.

The high-energy gap follows a BCS behavior with a ratio $2\Delta_2(0)/kT_c \approx 4.3$, significantly larger than the BCS value of 3.52. There are two possible sources for this increase. Usually such enhancement is attributed to strong coupling effect. However, this ratio also increases due to the presence of additional superconducting bands even in the weak coupling limit. In the case of $\Delta_1 \ll \Delta_2$ one can derive a simple formula from the two-band BCS theory

$$\frac{2\Delta_2}{T_c} \approx 3.52 \left(1 + \frac{N_1 \Delta_1^2}{N_2 \Delta_2^2} \ln \frac{\Delta_2}{\Delta_1} \right).$$

Using $N_2 = 0.73N_1$ from [2] and experimental values of the gaps, we estimate from this formula $2\Delta_2/T_c \approx 4.1$. Therefore, we conclude that the main part of the $2\Delta/T_c$ increase originates from the multiband nature of the superconductivity in this compound.

Finally, we would like to point out that in the case of two-band superconductivity in the dirty limit ($l \ll \xi$) the conductance spectra are very broad and similar to those reported earlier [8]. These spectra are mostly obtained on pellets without any surface treatment. Impurities near the surface may provide sufficiently strong interband scattering to smear out the two-gap features in this case.

In conclusion, the existence of two gaps has been observed by tunneling spectroscopy in compact pellets of MgB₂. Tunneling spectra show different ratios between the two gap heights on different grains within the sample. This result can be interpreted in terms of different tunneling directions with respect to the crystallographic orientation of the grain, therefore supporting the two-gap scenario [2,15]. Different tunneling direction should probe the two bands with different weights. Moreover, the two gaps both vanish at a temperature close to the bulk value. The observed temperature independence of the small gap up to $T \approx 20$ K implies that no transition temperature corresponding to the BCS ratio $2\Delta_1=3.52 kT_c$ is present. This suggests that the coupling between the two bands is moderately strong and that the superconductivity is dominant in the 2D sheets.

This work was supported by US DOE Basic Energy Science - Material Science under contract No. W-31-109-ENG-38.

-
- [1] H. Suhl, B. T. Matthias, and L. R. Walker, Phys. Rev. Lett. **3**, 552 (1959)
 - [2] A. Y. Liu, I. I. Mazin, and J. Kortus, Phys. Rev. Lett. **87**, 87005 (2001)
 - [3] J. Nagamatsu, N. Nakagawa, T. Muranaka, Y. Zenitani, and J. Akimitsu, Nature **410**, 63 (2001)
 - [4] F. Bouquet, R. A. Fisher, N. E. Phillips, and D. J. Hinks cond-mat/0104206

- [5] Y. Wang, T. Plackonwski, and A. Junod, *Physica* **355C**, 179 (2001)
- [6] S. L. Bud'ko *Phys. Rev. Lett.* **86**, 1877 (2001)
- [7] D. J. Hinks, H. Claus, and J. D. Jorgensen, *Nature* **411**, 458 (2001)
- [8] G. Karapetrov, M. Iavarone, W. K. Kwok, G. W. Crabtree, and D. G. Hinks, *Phys. Rev. Lett.* **46**, 4374 (2001)
- [9] G. Rubio-Bollinger, H. Suderow, and S. Vieira, *Phys. Rev. Lett.* **86**, 5582 (2001)
- [10] H. Schmidt, J. F. Zasadzinski, K. E. Gray, D. G. Hinks, *Phys. Rev. B* **63**, 220504 (2001)
- [11] F. Giubileo, D. Roditchev, W. Sacks, R. Lamy, D.X. Thanh, J. Klein, S. Miraglia, D. Fruchart, J. Marcus, and Ph. Monod, *Phys. Rev. Lett.* **87**, 177008 (2001)
- [12] P. Szabo, P. Samuely, J. Kacmarcik, T. Klein, J. Marcus, D. Fruchart, S. Miraglia, C. Mercenat, and A. G. M. Jansen, *Phys. Rev. Lett.* **87**, 137005 (2001)
- [13] H. Schmidt, J. F. Zasadzinski, K. E. Gray, D. G. Hinks, *cond-mat/0112144* (2002)
- [14] X. K. Chen, M. J. Konstantinovic, J. C. Irwin, D. D. Lawrie, and J. P. Franck, *cond-mat/0104005*
- [15] H. J. Choi, D. Roundy, H. Sun, M. L. Cohen, and G. Louie, *cond-mat/0111183*
- [16] R. J. Olsson, W. K. Kwok, G. Karapetrov, M. Iavarone, H. Claus, C. Peterson, G. W. Crabtree, W. N. Kang, H. J. Kim, E. M. Choi and S. I. Lee, *cond-mat/0201022*
- [17] Band structure calculations by Liu et al. actually show that MgB_2 has four bands, two 3D bands and two quasi-2D bands. We assume that the interband impurity scattering effectively mixes 3D bands and 2D bands, so that the system can be described by only two gap parameters, one (smaller) for two 3D bands and another (larger) for two 2D bands.
- [18] C. C. Sung and V. K. Wong, *J. Phys. Chem. Sol.*, **28**, 1933 (1967)
- [19] A. A. Golubov and I. I. Mazin, *Phys. Rev. B*, **55**, 15146 (1997)
- [20] N. Schopohl and K. Scharnberg, *Solid State Commun.* **22**, 371 (1977)

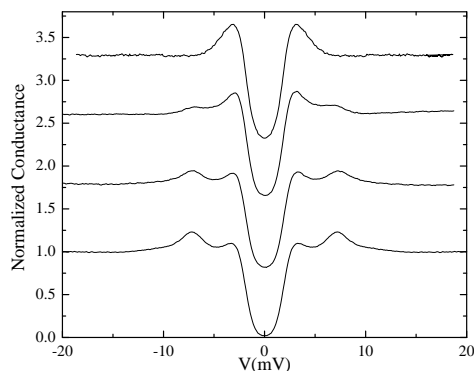


FIG. 1. Tunneling conductance spectra recorded on different grains at $T=4.2\text{K}$. The tunneling resistance is $0.2\text{ G}\Omega$. The spectra have been normalized to the conductance value at high voltage.

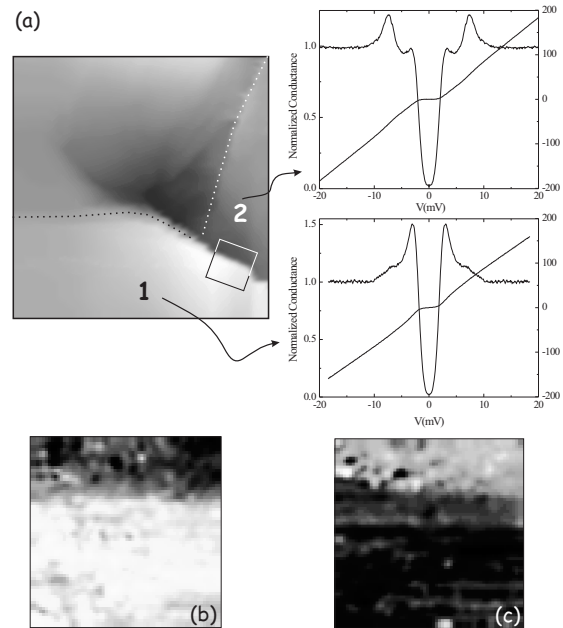


FIG. 2. (a) Topographic image of the scanning area $150\text{ nm} \times 150\text{ nm}$ acquired in the constant current mode (sample bias $V = -20\text{ mV}$, $I = 200\text{ pA}$). The conductance spectra and the current-voltage characteristics on two different grains are shown on the right. The tunneling resistance is $0.2\text{ G}\Omega$. (b) and (c) Conductance maps of the scanning area $30\text{ nm} \times 30\text{ nm}$ outlined in image (a) by the square across the grain boundary. The conductance maps have been recorded at $V_1=3.3\text{ mV}$ (b) and $V_2=7.3\text{ mV}$ (c) respectively.

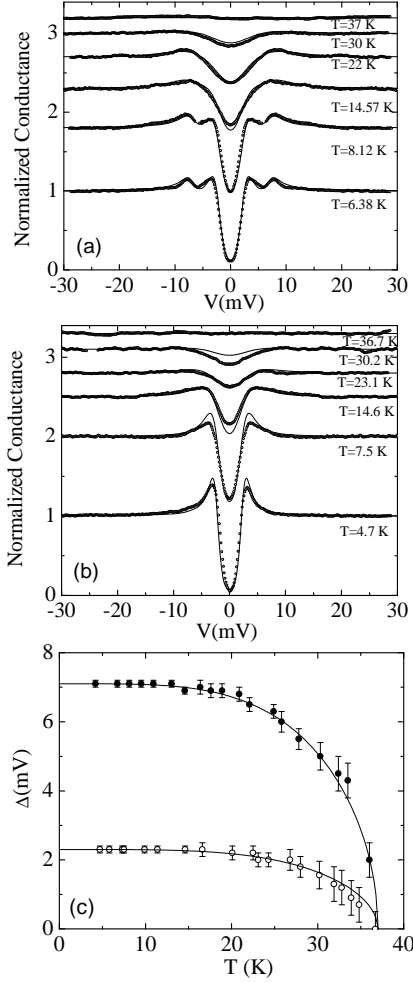


FIG. 3. Temperature evolution of the two tunneling spectra together with the theoretical curves. For all the curves $\Gamma_{12}=0.1$ mV, $\Gamma_{21}=0.14$ mV, $\Gamma=0.11$ mV (values optimized to the experimental curves at 4.2 K). In (a) the curves are reproduced using $\alpha=0.87$, $\beta=0.13$. In (b) $\alpha=1$, $\beta=0$. In (c) the gap values are extracted from the theoretical curves and are plotted as a function of the temperature together with the BCS $\Delta(T)$.